ADVANCED HEALTHCARE MATERIALS
www.advhealthmat.de

3D Interconnected Mesoporous Alumina with Loaded Hemoglobin as a Highly Active Electrochemical Biosensor for H_2O_2

Xuanyu Yang, Xiaowei Cheng, Hongyuan Song, Junhao Ma, Panpan Pan, Ahmed A. Elzatahry, Jiacan Su,* and Yonghui Deng**

Alumina is one of the most common and stable metal oxides in nature, which has been developed as a novel adsorbent in enrichment of biomolecules due to its excellent affinity to phosphor or amino groups. In this study, ordered mesoporous alumina (OMA) with interconnected mesopores and surface acidic property is synthesized through a solvent evaporation induced co-assembly process using poly(ethylene oxide)-*b*-polystyrene (PEO-*b*-PS) diblock copolymer as a template and aluminium acetylacetonate ($Al(acac)_3$) as the aluminium source. The pore size (12.1–19.7 nm), pore window size (3.5–9.0 nm) and surface acidity (0.092–0.165 mmol g^{-1}) can be precisely adjusted. The highly porous structure endows the OMA materials with high hemoglobin (Hb) immobilization capacity (170 mg g^{-1}). The obtained Hb@OMA composite is used as an electrocatalyst of biosensor for convienet and fast detection of hydrogen peroxide (H_2O_2) with a low H_2O_2 detection limit of 1.7×10^{-8} M and a wide linear range of 2.5×10^{-8} to 5.0×10^{-5} M. Moreover, the Hb@OMA sensors show a good performance in real time detection of H_2O_2 released from Homo sapiens bone osteosarcoma, indicating their potential application in complex biological processes.

Hydrogen peroxide (H_2O_2) is one of the most important representatives among the sources of reactive oxygen species.[1] It plays a significant role in many biological consumption processes within the living cells.[2] Since the abnormal metabolism of reactive oxygen species can bring about irreversible damages to the living cells, some common illnesses, such as cardiovascular disease, Alzheimer's disease and cancer, could be caused by the excess reactive oxygen species in human body.[3] Therefore, the rapid and accurate detection to H_2O_2 is of great significance in performing disease warning as early as possible and bringing to light the intimate relationships of H_2O_2 and human health. Numerous analytical methods have been explored to detect H_2O_2 concentration, such as titrimetry,[4] photometry,[5] chemiluminescence,[6] high-performance liquid chromatography,[7] and electrochemistry.[8] During the past few years, the electrochemical sensors for H_2O_2 detection have attracted more and more attention, owing to their simple operation, fast response, and low detection limit.[9] Particularly, electrochemical sensors based on biocatalysts with integrated active biomacromolecules have attracted much attention due to their advantage of high stereo-, chemo-, and regioselectivity and environmentally friendliness.[10]

Considerable efforts have been made to fabricate electrochemical biosensors by using surfactants,[11] polymers,[12] quantum dots,[13] porous materials,[8a,14] and so on. Ordered mesoporous materials (OMMs) have shown great potentials in

X. Yang, X. Cheng, J. Ma, Prof. Y. Deng
Department of Chemistry
State Key Laboratory of Molecular Engineering of Polymers
Shanghai Key Laboratory of Molecular Catalysis
and Innovative Materials
*i*ChEM
Fudan University
Shanghai 200433, China
E-mail: xwcheng@fudan.edu.cn; yhdeng@fudan.edu.cn

H. Song, P. Pan, Prof. J. Su
Department of Ophthalmology
Changhai Hospital
Second Military Medical University
Shanghai 200433, China
E-mail: drsujiacan@163.com

Prof. A. A. Elzatahry
Materials Science and Technology Program
College of Arts and Sciences
Qatar University
Doha 2713, Qatar

Prof. Y. Deng
State Key Lab of Transducer Technology
Shanghai Institute of Microsystem and Information Technology
Chinese Academy of Sciences
Shanghai 200050, China

The ORCID identification number(s) for the author(s) of this article can be found under https://doi.org/10.1002/adhm.201800149.

DOI: 10.1002/adhm.201800149

various fields such as separation,[15] adsorption,[16] catalysis,[17] and energy conversion and storage[18,19] due to their outstanding physicochemical properties (i.e., high specific surface area, large pore volume, tunable pore diameter, pore structure, and framework composition), which are beneficial to mass diffusion, high dispersion of active species, and stable immobilization of biomolecules in the mesopores.[20] In comparison with the OMMs with 1D pore structure, greatly restricting the diffusion of biomacromolecules such as enzymes by blocking of pore mouth, the OMMs with 3D interconnected mesopores provide open diffusion channels and rich anchoring sites for enzymes, which can eventually enhance their activity and stability and prohibit the leaching potentials out of mesostructures.[21] Moreover, besides the pore structures, the other characteristics of OMMs, such as the surface acidity and the complicated interactions between supports and enzymes, can also have distinct effects on mass diffusion and enzyme immobilization.[10,22] Therefore, the efficiency of biocatalyst can be enhanced by precisely optimizing the immobilization of enzymes in OMMs with large specific surface area and pore volume and suitable surface.[20]

In recent years, various metal oxides, such as TiO_2, WO_3, Nb_2O_5, ITO, and Al_2O_3, have been demonstrated as emerging supporting matrices in electrochemical detection of H_2O_2.[8a,14a,23,24] Among these metal oxides, Al_2O_3 has been considered to be particularly promising candidate because it has good stability and excellent affinity to biomolecules (e.g., proteins and enzymes).[25,26] Al_2O_3 materials with disordered pores have been used to support biomacromolecular hemoglobin molecules (molecular dimension $5.3 \times 5.4 \times 6.5$ nm) for electrochemical detection of H_2O_2. However, due to the poorly connected disordered pores, these Al_2O_3 materials mainly adsorb Hb on external surface, leading to a narrow linear range (1.9×10^{-7} to 2.0×10^{-5} M), relatively high detection limit, and possible abscission of Hb.[14a] Therefore, the comprehensive performance, including the stability of the sensor need to be improved from a viewpoint of practical applications. However, to our knowledge, little work has been done to rationally design and synthesize ordered mesoporous alumina with tunable pore parameters, such as pore diameter, pore window size, and the acidity of pore wall, so as to develop high-performance electrocatalyst of biosensor for detection of hydrogen peroxide.

Herein, we synthesized highly ordered mesoporous Al_2O_3 through a solvent evaporation induced coassembly (EICA) pathway using poly(ethylene oxide)-*b*-polystyrene (PEO-*b*-PS) diblock copolymers as the soft template and aluminium acetylacetonate ($Al(acac)_3$) as the aluminium source with high specific surface area and large pore volume with a face centered cubic (fcc) mesoporous structure ($Fm\bar{3}m$). The ordered mesoporous Al_2O_3 can be readily tailored with pore size (12.1–19.7 nm), pore window sizes (3.5–9.0 nm), high surface area (78–175 $m^2\ g^{-1}$), and adjustable pore volume of 0.22–0.67 $cm^3\ g^{-1}$ by changing the molecule weight of PEO-*b*-PS and the feeding ratio of $Al(acac)_3$/PEO-*b*-PS in the precursor solution. The surface acidity (0.092–0.165 mmol g^{-1}) can be precisely adjusted by changing the calcination temperature. Due to the 3D interconnected pore structure and rich surface acidity, the ordered mesoporous Al_2O_3 provides enormous anchoring sites for Hb immobilization and the Hb@OMA composites can be further fabricated as an electrode to detect hydrogen peroxide (H_2O_2), an important indicator for the metabolism of reactive oxygen species in living cells. The Hb@OMA composite with a high loading capacity of Hb (170 mg g^{-1}) performs excellent electrocatalytic activity with superior performance of a wide linear range from 2.5×10^{-8} to 5.0×10^{-5} M and a low detection limit of 1.7×10^{-8} M (S/N = 3) which was estimated by using $3\sigma/b$ where σ is the standard deviation of the blank and b is the slope of the calibration curve. The Hb@OMA biosensors exhibited good stability and durable determination of H_2O_2. Moreover, the as-fabricated Hb@OMA sensors show excellent performance in real-time detection of ultralow concentration of H_2O_2 released from MG63 cells, which is important for bioanalysis in many biological processes.

The amphiphilic PEO-*b*-PS diblock copolymers with different PS length were prepared via the well-established atom transfer radical polymerization (ATRP) method[27] and used for the synthesis of OMA materials via EICA (**Figure 1**) approach, where PEO-*b*-PS copolymers act as the soft template, $Al(acac)_3$ and THF were used as the aluminum source and the solvent, respectively. The pH value of the mixture is controlled by introducing a certain amount of concentrated nitric acid (67 wt%). First, the water-insoluble PEO-*b*-PS was dissolved in an acidic THF/$Al(acac)_3$ solution. The aluminum hydroxide sol was formed through controllable hydrolysis of $Al(acac)_3$, due to the slow liberation of acetylacetone as a coordination ligand to dominate the condensation rate. The stabilized sols can strongly interact with the PEO segments of PEO-*b*-PS molecules by hydrogen bonding, which can prohibit phase separation of PEO-*b*-PS molecules and hydrolyzed aluminum sols. Upon the successive evaporation of THF, the PEO-*b*-PS molecules and inorganic precursors gradually aggregate into spherical micelles with hydrophobic PS blocks as the core and hydrophilic PEO segments with associated inorganic sol as the shell. Second, to achieve a minimum interface free energy, the organic–inorganic hybrid micelles stack closely and co-assemble into organic–inorganic composites with fcc ordered mesostructures. Third, the as-formed composite was first treated in N_2 at 600 °C, and then the OMA materials with different textural properties and acidity can be obtained by calcination in air to remove the template and promote the crystallization of Al_2O_3 framework. By using PEO-*b*-PS diblock copolymers with different molecular weight, a series of OMA samples were synthesized and denoted as OMA-PEO_X-*b*-PS_Y-Z, where X and Y stand for the number of repeating unit of the monomers of EO and styrene, respectively, and Z is the calcination temperature in air.

The wide-angle X-ray diffraction (XRD) patterns of OMA-PEO_{117}-*b*-PS_{220}-600 sample show a broad diffraction peak at around 25°, suggesting an amorphous framework of alumina (**Figure 2**A-a). The obtained OMA-PEO_{117}-*b*-PS_{220}-900 displayed seven well-resolved diffraction peaks (Figure 2A-b), which are exactly indexed to the 111, 220, 311, 222, 400, 511, and 440 reflections of γ-Al_2O_3 phase (JCPDS Card No. 10-0425), respectively. It implies that the amorphous alumina was converted into crystalline γ-Al_2O_3 phase after treatment at higher temperature of 900 °C. The small-angle X-ray scattering (SAXS) pattern of OMA-PEO_{117}-*b*-PS_{220}-600 (Figure 2B-a) exhibits four well-resolved scattering peaks at q values of 0.369, 0.653, 0.754, and 1.496 nm^{-1}, respectively, which can be indexed to the 111, 222, 400, and 533 reflections of a fcc mesostructure with the space group of $Fm\bar{3}m$. It indicates that the ordered

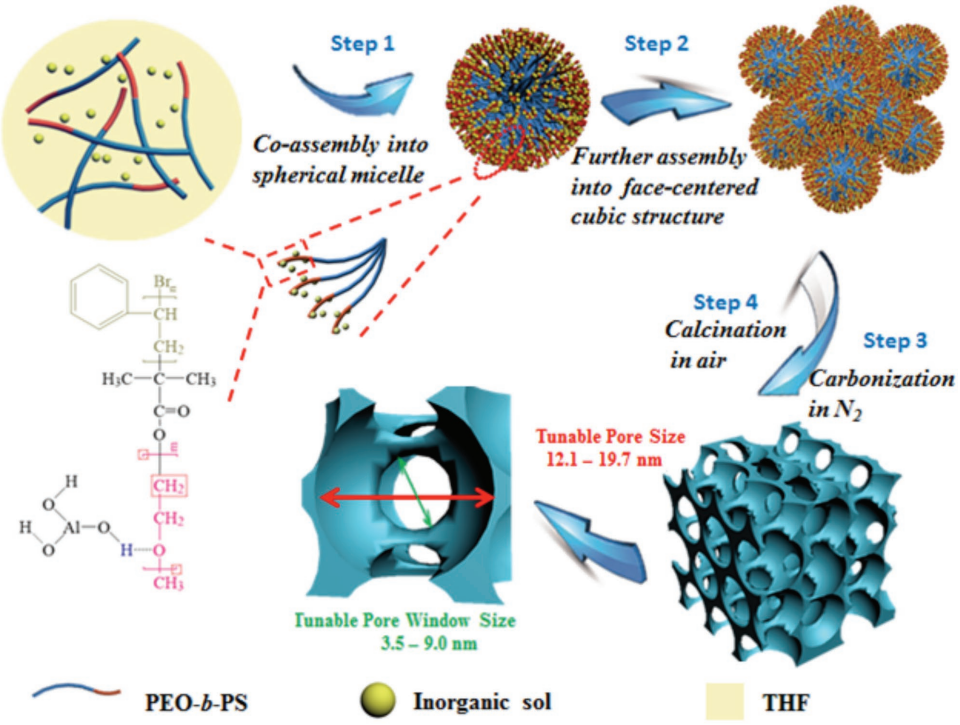

Figure 1. Scheme for the synthesis of ordered mesoporous Al_2O_3 by solvent evaporation induced coassembly process. Step 1: coassemble of alumina oligomers and PEO-*b*-PS into spherical micelles with the core of hydrophobic PS blocks and the shell of PEO segments during the evaporation of THF; Step 2: the spherical PEO-*b*-PS/inorganic sol composite micelles further aggregate into face-centered cubic mesostructures after complete evaporation of THF; Step 3: the formation of ordered mesostructures of carbon/Al_2O_3 composites by carbonization in N_2 atmosphere at 600 °C; Step 4: ordered mesoporous Al_2O_3 with large pores can be obtained by calcination in air to remove the carbon species.

cubic mesostructure was well retained after removal of the template. The sample of OMA-PEO_{117}-*b*-PS_{220}-900 obtained after calcination at 900 °C still presents four scattering peaks (Figure S1, Supporting Information), showing an ultrastable ordered mesostructure. The unit cell parameter decreases from 29.5 nm for OMA-PEO_{117}-*b*-PS_{220}-600 to 26.9 nm for OMA-PEO_{117}-*b*-PS_{220}-900 due to the structural shrinkage by calcination at higher temperature. Similar to OMA-PEO_{117}-b-PS_{220}-600, the SAXS patterns of OMA-PEO_{117}-*b*-PS_{182}-600 (Figure 2B-b) and OMA-PEO_{117}-*b*-PS_{130}-600 (Figure 2B-c) display four obvious scattering peaks with a shift to higher *q* values due to the smaller building blocks constructed by PEO-*b*-PS template with shorter hydrophobic PS chains (Figure 2B inset). Correspondingly, they have smaller unit cell parameters of 27.5 and 26.1 nm, respectively. Field-emission scanning electron microscope (FESEM) observation from the smooth surface (Figure 2C) and the cross section (Figure 2D) of OMA-PEO_{117}-*b*-PS_{220}-600 show highly ordered and uniform spherical mesopores over a large domain. After calcination in air at 900 °C, the highly ordered mesostructure was well retained in the OMA-PEO_{117}-*b*-PS_{220}-900 sample (Figure S2a, Supporting Information), in good agreement with the SAXS result (Figure S1, Supporting Information). Transmission electron microscopy (TEM) images of OMA-PEO_{117}-*b*-PS_{220}-600 (Figure 2E,F, Supporting Information) taken along the [100] and [211] directions reveal a highly ordered mesostructure with the typical fcc symmetry. By using PEO_{117}-*b*-PS_{182} and PEO_{117}-*b*-PS_{130} with shorter PS chains as the structure directing agent, the obtained OMA-PEO_{117}-*b*-PS_{182}-600 and OMA-PEO_{117}-*b*-PS_{130}-600 materials both possess highly ordered mesoporous structure and uniform spherical mesopores of 15.0 and 12.0 nm, respectively (Figures S3a,b and S4a,b, Supporting Information).

Nitrogen adsorption–desorption isotherms of OMA-PEO_{117}-*b*-PS_{220}-600 (**Figure 3**A) display typical type-IV curves with a sharp capillary condensation step in the relative pressure (P/P_0) of 0.85–0.95, indicating a highly uniform mesostructure with large pore size. The capillary condensation occurs at P/P_0 of 0.85 with H_1-type hysteresis loops, implying that the OMA materials possess cage-like mesopores. The pore size distribution (PSD) curve derived from the adsorption branch of the isotherms calculated by using Barrett–Joyner–Halenda (BJH) model reveals that the OMA-PEO_{117}-*b*-PS_{220}-600 sample has a uniform pore size of 19.7 nm (Figure 3B). The average pore window size is 9.0 nm, derived from the desorption branch using BJH model (Figure 3C). The specific surface area and pore volume of OMA-PEO_{117}-*b*-PS_{220}-600 were calculated to be 137 $m^2\ g^{-1}$ and 0.67 $cm^3\ g^{-1}$ (**Table 1**), respectively, indicating a rich porosity of the OMA materials. Even after calcination at 900 °C, the OMA-PEO_{117}-*b*-PS_{220}-900 sample shows similar N_2 adsorption–desorption isotherms (Figure S5, Supporting Information), except that the mesopore and pore window size slightly decrease to 17.8 and 5.5 nm, respectively, owing to the structure shrinkage and crystallization of alumina framework, and the specific surface area and pore volume were also reduced to 78 $m^2\ g^{-1}$ and 0.22 $cm^3\ g^{-1}$ (Table 1), respectively. In addition, OMA-PEO_{117}-*b*-PS_{182}-600 and OMA-PEO_{117}-*b*-PS_{130}-600 synthesized using templates with lower

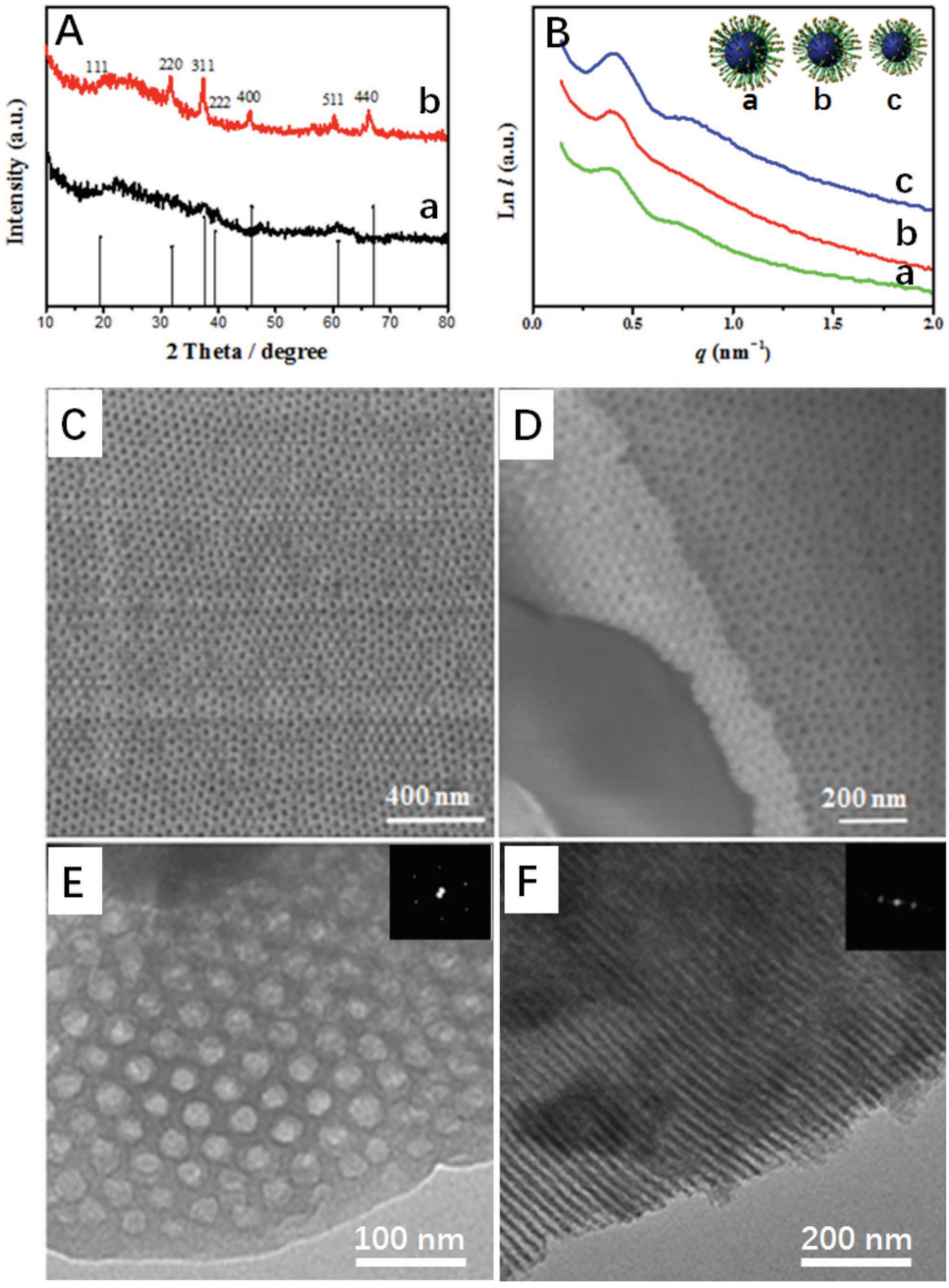

Figure 2. A) XRD patterns of OMA sample templated by PEO_{117}-*b*-PS_{220} after calcination in air at (a) 600 and (b) 900 °C. B) SAXS patterns of OMA-PEO_x-*b*-PS_y samples after calcination in air at 600 °C: (a) OMA-PEO_{117}-*b*-PS_{220}-600, (b) OMA-PEO_{117}-*b*-PS_{182}-600, and (c) OMA-PEO_{117}-*b*-PS_{130}-600. C) FESEM and TEM image of OMA-PEO_{117}-*b*-PS_{220}-600 taken along the directions of D) [100] and E) [211]. The insets are their corresponding fast Fourier transform (FFT).

Table 1. Textural properties and performance of H_2O_2 biosensing on the samples of OMA-PEO_x-*b*-PS_y.

Sample	Pore size [nm]	Window size [nm]	Surface area [$m^2\ g^{-1}$]	Pore volume [$cm^3\ g^{-1}$]	Acid amount [$mmol\ g^{-1}$]	Desorption temperature of NH_3[°C]	Hb Loading [$mg\ g^{-1}$]	Detection limit [M]	Linear range [M]
OMA-PEO_{117}-*b*-PS_{130}-600	12.1	3.5	175	0.41	0.143	167	140	7.9×10^{-8}	1.0×10^{-7}–1.0×10^{-5}
OMA-PEO_{117}-*b*-PS_{182}-600	15.1	4.5	161	0.36	0.141	163	120	2.0×10^{-7}	2.5×10^{-7}–1.0×10^{-4}
OMA-PEO_{117}-*b*-PS_{220}-600	19.7	9.0	137	0.67	0.165	188	170	1.7×10^{-8}	2.5×10^{-8}–5.0×10^{-5}
OMA-PEO_{117}-*b*-PS_{220}-900	17.8	5.5	78	0.22	0.092	191	110	3.5×10^{-7}	5.0×10^{-7}–5.0×10^{-5}

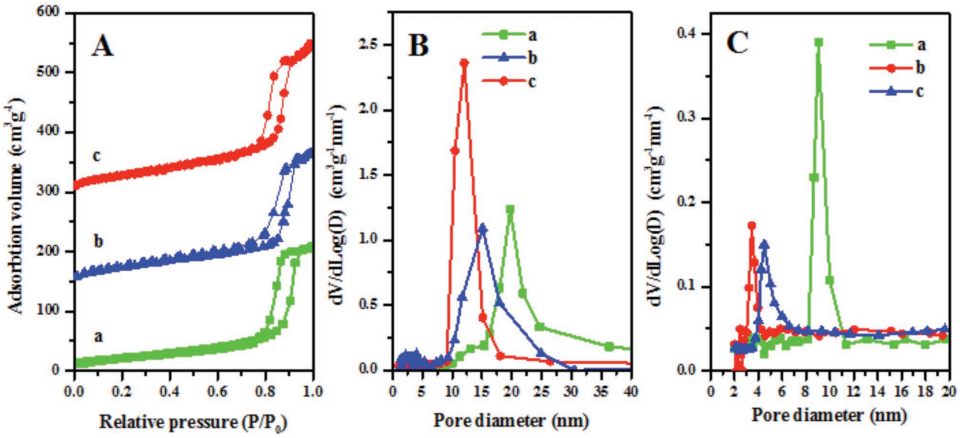

Figure 3. A) N_2 sorption isotherms, B) pore size distribution curves, and C) pore window size distribution curves of OMA-PEO_x-*b*-PS_y samples after calcination in air at 600 °C using different template: (a) OMA-PEO_{117}-*b*-PS_{220}-600, (b) OMA-PEO_{117}-*b*-PS_{182}-600, and (c) OMA-PEO_{117}-*b*-PS_{130}-600.

molecular weights show nitrogen adsorption–desorption isotherms similar to those of OMA-PEO_{117}-*b*-PS_{220}-600, indicating a similar coassembly process that leads to highly fcc mesostructured OMA materials. Their pore sizes are 15.1 and 12.1 nm, respectively, smaller than that of OMA-PEO_{117}-*b*-PS_{220}-600 (19.7 nm), but their specific surface areas are 160 m^2 g^{-1} and 175 m^2 g^{-1}, respectively, higher than that of OMA-PEO_{117}-*b*-PS_{220}-600 (Table 1). It is worth noting that, because PEO_{117}-*b*-PS_{220} coassemble with inorganic sols into large micelles during EICA, they further closely pack into ordered structure where the contacting area between the neighboring micelles is relatively large, which leads to OMA-PEO_{117}-*b*-PS_{220} with the largest window size among the above OMA samples.

Ammonia temperature programmed desorption (NH_3-TPD) experiments were conducted to study the surface acidity of the OMA materials obtained after calcination at different temperatures. Only one broad desorption peak appears at around 200 °C in the NH_3-TPD profiles of all the samples (Figure S6, Supporting Information). It can be attributed to the NH_3 chemically adsorbed on the Lewis acid sites,[28] which have been considered to be favorable for protein enrichment or enzyme immobilization in porous materials.[29] The sample OMA-PEO_{117}-*b*-PS_{220}-600 possesses the highest Lewis acid amount of 0.165 mmol g^{-1} among all OMA materials (Table 1), and its Lewis acid strength is close to OMA-PEO_{117}-*b*-PS_{182}-600 (0.141 mmol g^{-1}) and OMA-PEO_{117}-*b*-PS_{130}-600 (0.143 mmol g^{-1}), but higher than OMA-PEO_{117}-*b*-PS_{220}-900 (0.092 mmol g^{-1}). These results indicate that thermal treatment of mesoporous OMA materials at high temperature can cause further dehydration, decreasing the amount of surface hydroxyl groups and thus the surface acidity of OMA materials.

The highly 3D interconnected mesoporous structures with high surface area, large pores, and the intrinsic surface Lewis acidity of OMA materials make them a promising carrier for host–guest chemistry, such as loading biomacromolecules of large size, catalytically active nanoparticles, and enzymes.[30] Hemoglobin (Hb) with a dimension of 5.3 × 5.4 × 6.5 nm is an important heme protein with four polypeptide chains, each of which involves one electroactive iron heme group.[31] Because of its intrinsic catalytic activity toward H_2O_2, Hb has been extensively used as an ideal model molecule to study the direct electron transfer between electrode and heme protein. In order to enhance the stability and electrocatalytic activity of Hb molecules, porous support with interconnected pores larger than Hb is highly desired for loading Hb for electrochemical detection of H_2O_2. Herein, our large-pore OMA materials were used to load Hb via wet impregnation method. The adsorption of Hb on OMA materials was studied using UV–vis spectroscopy based on the characteristic absorption of Hb at 406 nm (Figure S7a,b, Supporting Information), and the Hb loading capacity was calculated to be 170 mg g^{-1} for OMA-PEO_{117}-*b*-PS_{220}-600, 140 mg g^{-1} for OMA-PEO_{117}-*b*-PS_{130}-600, 120 mg g^{-1} for OMA-PEO_{117}-*b*-PS_{182}-600, and 110 mg g^{-1} for OMA-PEO_{117}-*b*-PS_{220}-900, respectively (Table 1). The superior adsorption capacity of OMA-PEO_{117}-*b*-PS_{220}-600 can be ascribed to the 3D interconnected mesoporous structures with large pore and window size (9.0 nm) and large Lewis acid amount (0.165 mmol g^{-1}). Whereas, the lowest Hb loading capacity of OMA-PEO_{117}-*b*-PS_{220}-900 is caused by the low surface area (78 m^2 g^{-1}), low Lewis acid amount (0.092 mmol g^{-1}), and small pore window size (5.5 nm). The window size of cage-like mesopores is the most important factor in dominating Hb loading. Therefore, a rational control over the pore window size is extremely important for loading biomacromolecules in practical applications.

Due to its interconnected mesoporous structures with large pore window size (9.0 nm) and the large adsorption amount of Hb (170 mg g^{-1}), the as-fabricated Hb@OMA-PEO_{117}-*b*-PS_{220}-600 electrode was used as an electrochemical biosensor for H_2O_2 detection. The cyclic voltammograms of glass carbon electrodes (GCEs) modified with OMA-PEO_{117}-*b*-PS_{220}-600 show no obvious redox peaks (**Figure 4**A-a), implying that the OMA support is an electro-inactive matrix. However, in the case of Hb@OMA-PEO_{117}-*b*-PS_{220}-600 with immobilized Hb, the cathodic current changes dramatically and a distinct reduction peak appears at the potential of –0.32 V (Figure 4A-b), which stems from the fast electron transfer between Hb and electrode surface. Electrochemical performance of H_2O_2 reduction on Hb@OMA-PEO_{117}-*b*-PS_{220}-600 electrode as a biosensor was further investigated by cyclic voltammograms upon successive injection of H_2O_2 with different concentrations (Figure 4B). The reduction response currents increase gradually as the H_2O_2 concentration increases from 0 to 1.0×10^{-6} M, indicating the electrocatalytic reaction of the biosensor to H_2O_2 reduction.

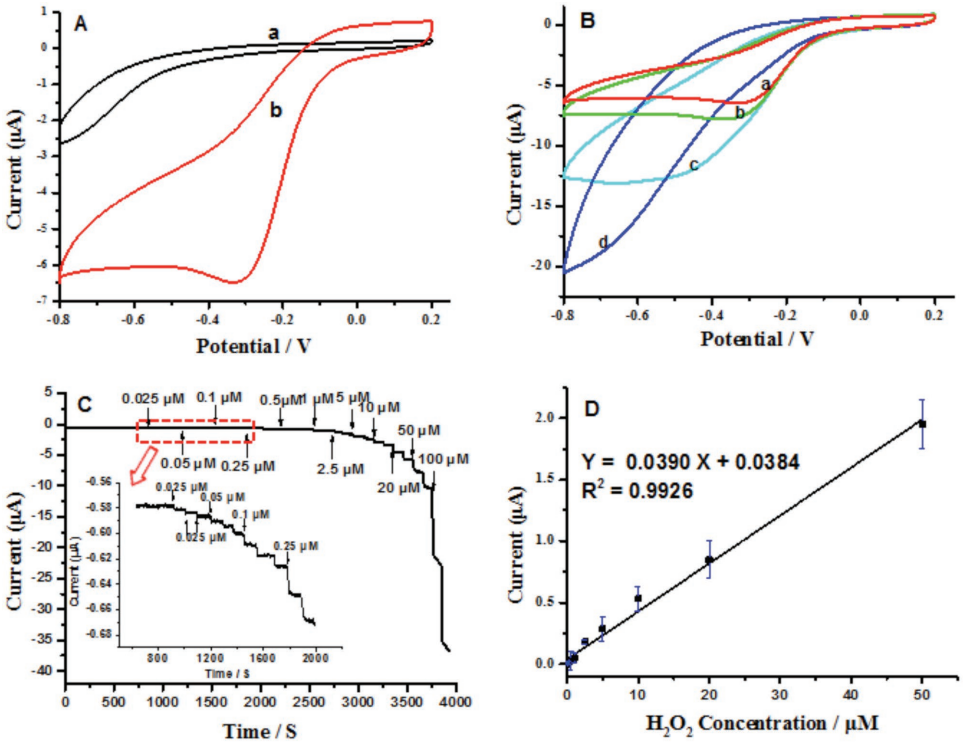

Figure 4. A) Cyclic voltammograms of OMA-PEO_{117}-*b*-PS_{220}-600 modified glassy carbon electrode before (a) and after (b) Hb immobilization. B) Cyclic voltammograms of Hb@OMA-PEO_{117}-*b*-PS_{220}-600 biosensor in H_2O_2 of different concentrations: (a) 0, (b) 0.1×10^{-6} M, (c) 0.25×10^{-6} M, (d) 1.0×10^{-6} M. C) Current–time responses of Hb@OMA-PEO_{117}-*b*-PS_{220}-600 biosensor to successive injections of H_2O_2 of different concentrations at an applied potential of –0.4 V. Inset: the current–time responses of low concentration region in enlarged view (from 25×10^{-9} to 0.25×10^{-6} M), and we have measured for three times at each concentration. D) The fitting plot of reduction current versus concentrations of H_2O_2 (from 25×10^{-9} to 50×10^{-6} M). Error bars refer to three replicates.

In order to evaluate the catalytic ability of Hb@OMA-PEO_{117}-*b*-PS_{220}-600 to H_2O_2 at micromolar level, the real-time amperometric response of stepwise change of H_2O_2 solutions was conducted by using chronoamperometry method. Upon adding H_2O_2 solutions with concentration of 2.5×10^{-8} to 5.0×10^{-5} M to the buffer solution under stirring, a stepwise growth of response current for H_2O_2 reduction can be clearly observed in the amperometric *I*–*t* curve (Figure 4C), and the reduction current sharply rises to 95% of the steady state in less than 10 s. These results suggest that the as-fabricated electrodes can be effectively used for durable and quick detection of H_2O_2. The response currents of the biosensor (Figure 4D) are linearly dependent on the concentration of H_2O_2 in the range of 2.5×10^{-8} to 5.0×10^{-5}M with a fitting equation as: I (μA) = 0.0384 + 0.0390 C (H_2O_2) (mM) (R^2 = 0.9926). The detection limit is calculated to be as low as 1.7×10^{-8}M (S/N = 3) using $3\sigma/b$, suggesting excellent performance in the detection of H_2O_2 at micromolar level. For comparison, OMA-PEO_{117}-*b*-PS_{220}-900, OMA-PEO_{117}-*b*-PS_{130}-600, and OMA-PEO_{117}-*b*-PS_{182}-600 with different acid amount, pore size, and window size of 4.5 nm (Table 1) were also employed to immobilize Hb for electrocatalytic detection of H_2O_2, which show inferior performance compared with Hb@OMA-PEO_{117}-*b*-PS_{220}-600 (Figures S3–S5, Supporting Information). The linear range of response current and detection limit which was estimated by using $3\sigma/b$ of the GCEs modified with Hb@OMA are 5.0×10^{-7} to 5.0×10^{-5} and 3.5×10^{-7} M (S/N = 3) of OMA-PEO_{117}-*b*-PS_{220}-900, 1.0×10^{-7} to 1.0×10^{-5} and 7.9×10^{-8} M (S/N = 3) of OMA-PEO_{117}-*b*-PS_{130}-600, and 2.5×10^{-7} to 1.0×10^{-4} and 2.0×10^{-7} M (S/N = 3) of OMA-PEO_{117}-*b*-PS_{182}-600, respectively, in which the biosensor of Hb@OMA-PEO_{117}-*b*-PS_{220}-600 exhibits the best performance for H_2O_2 detection (Table 1), and the excellent performance can be ascribed to the stable immobilization of Hb molecules and the facile diffusion of guest species in the matrix.

From the discussion above, the outstanding electrocatalytic performance of Hb@OMA-PEO_{117}-*b*-PS_{220}-600 biosensor in H_2O_2 detection can be well interpreted from the synergetic effects of specific mesostructures and surface activity. On one hand, the 3D interconnected pore structure with a large pore window size of 9.0 nm can enhance the diffusion and transport of guest species in mesopores to interact with anchoring sites for adsorption of Hb molecules (**Figure 5**). On the other hand, since OMA-PEO_{117}-*b*-PS_{220}-600 owns rich Lewis acidity and good biocompatibility, Hb molecules could be stably immobilized on alumina without damaging functions. To further explore the application possibility of our Hb@OMA-based sensor for detection of H_2O_2 in biosystem, a real-time detection of H_2O_2 in living cells was carried out using Hb@OMA-PEO_{117}-*b*-PS_{220}-600 electrode. The H_2O_2 released from MG63 cells (*Homo sapiens* bone osteosarcoma) was monitored by the Hb@OMA electrode and the release of H_2O_2 is triggered by injection of fMLP solution (N-formylmethionyl-leucyl-phenylalanine). The amperometric responses of Hb@OMA electrode to H_2O_2 in the presence and absence cells are shown in **Figure 6**. As the control, no obvious current change was observed in the

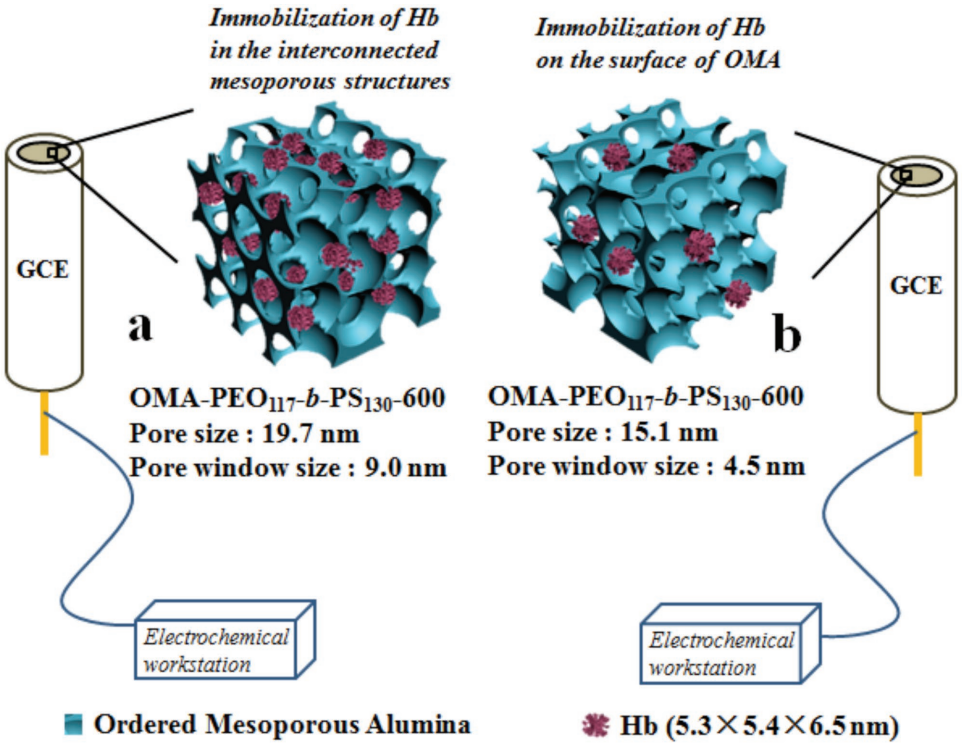

Figure 5. Schematic illustration of the hydrogen peroxide biosensing mechanism. a) Hb molecules are adsorbed in the interior of OMA material with large pore window size (>6 nm). b) Hb molecules are adsorbed on the surface of OMA material with small pore window size (<6 nm).

absence of cells under the same conditions (Figure 6A). After introduction of 300×10^{-9} and 600×10^{-9} M fLMP into the MG63 cells solution, the cathodic current suddenly increased (Figure 6B,C). The change of amperometric responses to the release of H_2O_2 from MG63 cells is roughly proportional to the addition amount of fLMP. Hereby, it can be deduced that the increase of current response in the presence of MG63 cells is ascribed to the release of H_2O_2 triggered by fLMP. The current change before and after addition of 600×10^{-9} M fLMP is around 0.07 μA. Therefore, it can be estimated that the maximum of H_2O_2 released from 5×10^6 MG63 cells is 0.81×10^{-6} M based on the equation: I (μA) = 0.0384 + 0.0390 C (H_2O_2) (mM) (R^2 = 0.9926). It can be expected that the as-fabricated Hb@OMA sensor can be used to reflect the metabolism of reactive oxygen species in living cells.

The stability of fabricated electrode was further investigated. The relative standard deviation (RSD) of current response of the Hb@OMA sensor to 0.2×10^{-6} M H_2O_2 is less than 1.5% for five measurements, indicating a reproducible H_2O_2 detection. The current response maintained at 93.9% of initial response after successive 50 cyclic voltammograms cycles of 1.0×10^{-6} M H_2O_2 (Figure S8, Supporting Information). After storing the fabricated Hb@OMA electrode at 25 °C for one month, the current response of the sensor to 0.2×10^{-6} M H_2O_2 retained at 91.3% of original value. These results confirmed the good stability of the fabricated electrode for H_2O_2 detection due to the stably immobilized Hb in the 3D interconnected mesoporous networks with large pore window size and rich Lewis acidity.

In summary, highly ordered mesoporous alumina with 3D interconnected and tunable large pores and pore window size and surface acidic property was rationally synthesized via a solvent evaporation induced coassembly approach by using lab-made amphiphilic diblock copolymer of PEO-*b*-PS with different

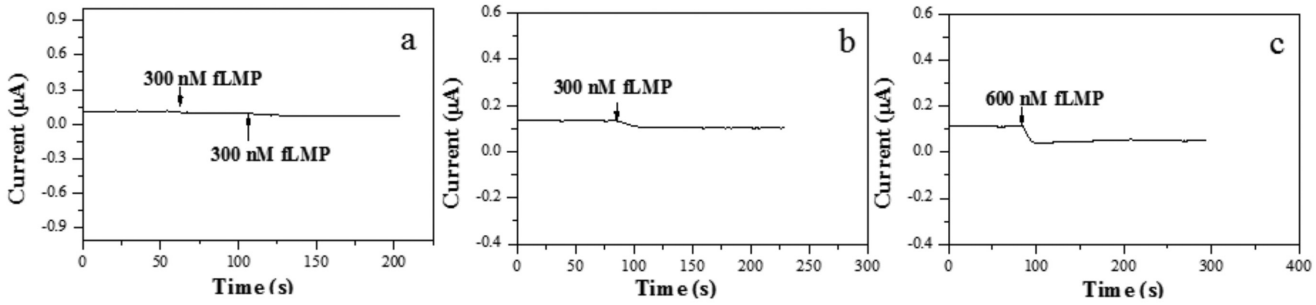

Figure 6. Current–time responses of H_2O_2 released from a) MG63 cells as well as b) without MG63 cells upon injections of 300×10^{-9} M fMLP and c) upon injections of 600×10^{-9} M fMLP.

chain length of PS, changing the $Al(acac)_3$/PEO-*b*-PS weight ratio and calcination temperature. By utilizing the 3D interconnected mesoporous alumina as the host for loading hemoglobin, a high-performance Hb@OMA electrocatalyst was fabricated, which was demonstrated to exhibit superior performance for electrochemical biosensing of H_2O_2 with a wide linear range from 25×10^{-9} to 50×10^{-6} M, a low detection limit of 1.7×10^{-8} M, fast response time (<15 s), and good reproducibility and stability. Moreover, the Hb@OMA biosensors show an excellent performance in real-time detection of ultralow concentration H_2O_2 (0.81×10^{-6} M) released from MG63 cells. Its outstanding electrocatalytic behaviors are mainly attributed to the stable immobilization of Hb molecules and the facile diffusion of guest species in the matrix. It is expected that the hybrid material can be used as an important biosensor in many biological processes.

Supporting Information

Supporting Information is available from the Wiley Online Library or from the author.

Acknowledgements

This work was supported by the NSF of China (51372041, 51422202, 21673048, 91749204 and 81771491), Shanghai Pujiang Program, China (No. 16PJ1401100), Key Basic Research Program of Science and Technology Commission of Shanghai Municipality (17JC1400100), Shanghai Municipal Science and Technology Commission Key Program (15411950600), Youth Top-notch Talent Support Program of China, the state key laboratory of Transducer Technology of China (Grant No. SKT1503), the Outstanding Talents Cultivation Program of Shanghai Health System (2017BR011), and Qatar University under GCC Co-Fund Program, Grant GCC-2017-001. The authors thank Prof. Guangrong Zhou for assistance in TEM characterization.

Conflict of Interest

The authors declare no conflict of interest.

Keywords

biosensors, electrocatalysts, hemoglobin, hydrogen peroxide, immobilization, porous alumina

Received: February 8, 2018
Published online:

[1] a) W. Maruyama, P. Dostert, K. Matsubara, M. Naoi, *Free Radical Biol. Med.* **1995**, *19*, 67; b) H. Ohshima, M. Tatemichi, T. Sawa, *Arch. Biochem. Biophys.* **2003**, *417*, 3.
[2] a) S. G. Rhee, *Science* **2006**, *312*, 1882; b) E. A. Veal, A. M. Day, B. A. Morgan, *Mol. Cell* **2007**, *26*, 1.
[3] a) F. Pagliari, C. Mandoli, G. Forte, E. Magnani, S. Pagliari, G. Nardone, S. Licoccia, M. Minieri, P. D. Nardo, E. Traversa, *ACS Nano* **2012**, *6*, 3767; b) P. Wu, Z. Cai, Y. Gao, H. Zhang, C. Cai, *Chem. Commun.* **2011**, *47*, 11327.
[4] N. V. Klassen, D. Marchington, H. C. E. Mcgowan, *Anal. Chem.* **1994**, *66*, 2921.
[5] A. Lobnik, M. Čajlaković, *Sens. Actuators, B* **2001**, *74*, 194.
[6] L. S. Zhang, G. T. F. Wong, *Talanta* **1999**, *48*, 1031.
[7] S. Effkemann, U. Pinkernell, U. Karst, S. Effkemann, U. Pinkernell, U. Karst, *Anal. Chim. Acta* **1998**, *363*, 97.
[8] a) W. Luo, Y. Li, J. Dong, J. Wei, J. Xu, Y. Deng, D. Zhao, *Angew. Chem., Int. Ed.* **2013**, *52*, 10505; b) L. Ren, J. Dong, X. Cheng, J. Xu, P. Hu, *Microchim. Acta* **2013**, *180*, 1333.
[9] B. J. Privett, J. H. Shin, M. H. Schoenfisch, *Anal. Chem.* **2010**, *82*, 4723.
[10] D. N. Tran, K. J. Balkus, *ACS Catal.* **2011**, *1*, 956.
[11] X. He, L. Zhu, *Electrochem. Commun.* **2006**, *8*, 615.
[12] a) Q. Lu, T. Zhou, S. Hu, *Biosens. Bioelectron.* **2007**, *22*, 899; b) H. Liu, Z. Tian, Z. Lu, Z Zhang, M. Zhang, D. Pang, *Biosens. Bioelectron.* **2004**, *20*, 294.
[13] Q. Lu, S. Hu, D. Pang, Z. He, *Chem. Commun.* **2005**, *0*, 2584.
[14] a) J. Yu, J. Ma, F. Zhao, B. Zeng, *Electrochim. Acta* **2007**, *53*, 1995; b) Y. Dai, H. Li, D. Wu, R. Li, Y. Zhao, B. Liu, Y. Cai, M. Yang, B. Du, Q. Wei, *Electroanalysis* **2011**, *23*, 1602; c) L. Zhang, S. Qiao, Y. Jin, Z. Chen, H. Gu, G. Lu, *Adv. Mater.* **2008**, *20*, 805; d) Z. Mu, J. Li, Z. Hao, S. Qiao, *Microporous Mesoporous Mater.* **2008**, *113*, 72; e) Z. Mu, J. Li, H. Tian, Z. Hao, S. Qiao, *Mater. Res. Bull.* **2008**, *43*, 2599; f) V. Malgras, H. Ataee-Esfahani, H. Wang, B. Jiang, C. Li, K. Wu, J. Kim, Y. Yamauchi, *Adv. Mater.* **2015**, *28*, 993; g) Y. Yamauchi, A. Sugiyama, R. Morimoto, A. Takai, K. Kuroda, *Angew. Chem., Int. Ed.* **2008**, *47*, 5371; h) Y. Hu, K. Qian, P. Yuan, Y. Wang, C. Yu, *Mater. Lett.* **2011**, *65*, 21; i) A. Lu, A. Kiefer, W. Schmidt, F. Schüth, *Chem. Mater.* **2004**, *16*, 100.
[15] Y. Liu, D. Shen, G. Chen, A. A. Elzatahry, M. Pal, H. Zhu, L. Wu, J. Lin, D. Al-Dahyan, W. Li, D. Zhao, *Adv. Mater.* **2017**, *29*, 1702274.
[16] X. Zhuang, Y. Wan, C. Feng, Y. Shen, D. Zhao, *Chem. Mater.* **2009**, *21*, 706.
[17] a) N. Parsafard, M. H. Peyrovi, N. Parsafard, *Chin. Chem. Lett.* **2017**, *28*, 546; b) B. Ji, Z. Qiao, I. Lee, M. Dahl, F. Zaera, Y. Yin, *Adv. Funct. Mater.* **2012**, *22*, 166; c) M. Kalantari, M. Yu, Y. Yang, E. Strounina, Z. Gu, X. Huang, J. Zhang, H. Song, C. Yu, *Nano Res.* **2017**, *10*, 605.
[18] W. Li, J. Liu, D. Zhao, *Nat. Rev. Mater.* **2016**, *1*, 16023.
[19] M. X. Ma, *Chin. Chem. Lett.* **2012**, *23*, 949.
[20] Z. Zhou, M. Hartmann, *Chem. Soc. Rev.* **2013**, *42*, 3894.
[21] L. Washmon, *J. Mol. Catal. B: Enzym.* **2000**, *10*, 453.
[22] R. A. Sheldon, *Adv. Synth. Catal.* **2007**, *349*, 1289.
[23] a) E. Topoglidis, C. J. Campbell, A. E. G. Cass, J. R. Durrant, *Electroanalysis* **2006**, *18*, 882; b) J. Feng, J. Xu, H. Chen, *Electrochem. Commun.* **2006**, *8*, 77.
[24] S. Frasca, T. von Graberg, J. Feng, A. Thomas, B. M. Smarsly, I. M. Weidinger, F. W. Scheller, P. Hildebrandt, U. Wollenberger, *ChemCatChem* **2010**, *2*, 839.
[25] a) S. Tan, B. Hu, W.G. Kim, S. H. Pang, J. S. Moore, Y. Liu, R. S. Dixit, J. G. Pendergast, D. S. Sholl, S. Nair, C. W. Jones, *ACS Catal.* **2016**, *6*, 5673; b) H. Ham, J. Kim, S. J. Cho, J.-H. Choi, D. J. Moon, J. W. Bae, *ACS Catal.* **2016**, *6*, 5629; c) C. Gunathilake, M. Gangoda, M. Jaroniec, *Ind. Eng. Chem. Res.* **2016**, *55*, 5598.
[26] A. Walcarius, A. Kuhn, *TrAC, Trends Anal. Chem.* **2008**, *27*, 593.
[27] Y. Deng, T. Yu, Y. Wan, Y. Shi, Y. Meng, D. Gu, L. Zhang, Y. Huang, C. Liu, X. Wu, *J. Am. Chem. Soc.* **2007**, *129*, 1690.
[28] J. Liu, C. Liu, A. Ma, J. Rong, Z. Da, A. Zheng, L. Qin, *Appl. Surf. Sci.* **2016**, *368*, 233.
[29] H. K. Kweon, K. Håkansson, *Anal. Chem.* **2006**, *78*, 1743.
[30] A. Vinu, V. Murugesan, O. Tangermann, M. Hartmann, *Chem. Mater.* **2004**, *16*, 3056.
[31] S. Peng, Q. Gao, Q. Wang, J. Shi, *Chem. Mater.* **2004**, *16*, 2675.